Automatica 174 (2025) 112184

Contents lists available at ScienceDirect

Automatica

journal homepage: www.elsevier.com/locate/automatica

A frequency domain analysis of slow coherency in networked systems☆

Hancheng Min [a,*], Richard Pates [b], Enrique Mallada [c]

[a] Electrical and Systems Engineering, University of Pennsylvania, Philadelphia, PA, USA
[b] Department of Automatic Control, Lund University, Lund, Sweden
[c] Electrical and Computer Engineering, Johns Hopkins University, Baltimore, MD, USA

ARTICLE INFO

Article history:
Received 16 February 2023
Received in revised form 6 December 2024
Accepted 1 January 2025
Available online 4 February 2025

Keywords:
Multi-agent systems
Large-scale networks
Slow coherency
Linear/nonlinear model
Low-rank approximation

ABSTRACT

Network coherence generally refers to the emergence of simple aggregated dynamical behaviors, despite heterogeneity in the dynamics of the subsystems that constitute the network. In this paper, we develop a general frequency domain framework to analyze and quantify the level of network coherence that a system exhibits by relating coherence with a low-rank property of the system's input–output response. More precisely, for a networked system with linear dynamics and coupling, we show that, as the network's *frequency-dependent algebraic connectivity* grows, the system transfer matrix converges to a rank-one transfer matrix representing the coherent behavior. Interestingly, the non-zero eigenvalue of such a rank-one matrix is given by the harmonic mean of individual nodal dynamics, and we refer to it as coherent dynamics. Our analysis unveils the frequency-dependent nature of coherence and a non-trivial interplay between dynamics and network topology. We further show that many networked systems can exhibit similar coherent behavior by establishing a concentration result in a setting with randomly chosen individual nodal dynamics.

1. Introduction

The study of coordinated behavior in network systems has been a popular subject of research in many fields, including physics (Bressloff & Coombes, 1999), chemistry (Kiss, Zhai, & Hudson, 2002), social sciences (DeGroot, 1974), and biology (Mirollo & Strogatz, 1990). Within engineering, coordination is essential for the proper operation of many networked systems, including power networks (Jiang, Pates, & Mallada, 2017; Paganini & Mallada, 2020), data and sensor networks (Mallada, 2014; Mallada, Meng, Hack, Zhang, & Tang, 2015), and autonomous transportation (Bamieh, Jovanovic, Mitra, & Patterson, 2012; Jadbabaie, Lin, & Morse, 2003; Olfati-Saber, Fax, & Murray, 2007; Sepulchre, Paley, & Leonard, 2008). Among many forms of coordination, *coherence* refers to the ability of a group of nodes to have a similar dynamic response to some external disturbance (Chow, 2013). While coherence analysis is useful in understanding the collective behavior of large networks, little do we know about the underlying mechanism that causes such coherent behavior to emerge in various networks.

Classic slow coherency analyses (Chow, 1982; Ramaswamy et al., 1996; Romeres et al., 2013; Tyuryukanov et al., 2021) (with applications mostly to power networks) usually consider the second-order electro-mechanical model without damping: $\ddot{x} = -M^{-1}Lx$, where M is the diagonal matrix of machine inertias, and L is the Laplacian matrix whose elements are synchronizing coefficients between pair of machines. The coherency or synchrony (Ramaswamy et al., 1996) (a generalized notion of coherency) is identified by studying the first few slowest eigenmodes (eigenvectors with small eigenvalues) of $M^{-1}L$. The analysis can be carried over to the case of uniform (Chow, 1982) and non-uniform (Romeres et al., 2013) damping. However, such state-space-based analysis is limited to very specific node dynamics (second order) Moreover, it is widely known that such coherence is related to strong interconnection among the nodes, such relation is not formally justified in the aforementioned slow coherency analyses.

A vast body of work, triggered by the seminal paper (Bamieh et al., 2012), has quantitatively studied the role of the network topology in the emergence of coherence. Examples include, directed (Tegling et al., 2019) and undirected (Oral et al., 2017) consensus networks, transportation networks (Bamieh et al., 2012), and power networks (Andreasson et al., 2017; Bamieh & Gayme, 2013; Paganini & Mallada, 2020; Pirani et al., 2017; Tegling et al., 2015). The key technical approach amounts to quantifying the level of coherence by computing the $\mathcal{H}_2$-norm of the system for appropriately defined nodal disturbance and performance signals. Broadly speaking, the analysis shows a reciprocal dependence

☆ The material in this paper was partially presented at the 58th IEEE Conference on Decision and Control, December 11–13, 2019, Nice, France. This paper was recommended for publication in revised form by Associate Editor Julien M. Hendrickx under the direction of Editor Christos G. Cassandras.

* Corresponding author.
E-mail addresses: hanchmin@seas.upenn.edu (H. Min), richard.pates@control.lth.se (R. Pates), mallada@jhu.edu (E. Mallada).

https://doi.org/10.1016/j.automatica.2025.112184
0005-1098/

Table 1
Comparison with prior work.

	References	Nodal dynamics	Input Signal	Coherent dynamics	Time-domain Bounds
Slow Coherency, Synchrony	Chow (1982), Ramaswamy et al. (1996), Romeres, Dörfler, and Bullo (2013), Tyuryukanov, Popov, van der Meijden, and Terzija (2021)	First- or second-order LTI; Heterogeneous	Any	✔	✗
$\mathcal{H}_2$-Analysis	Bamieh et al. (2012), Siami and Motee (2014)	LTI; Heterogeneous	White Noise	✗	✔
	Andreasson, Tegling, Sandberg, and Johansson (2017), Bamieh and Gayme (2013), Oral, Mallada, and Gayme (2017), Pirani, Shahrivar, and Sundaram (2015), Tegling, Bamieh, and Gayme (2015), Tegling, Bamieh, and Sandberg (2019)	LTI; Homogeneous	White Noise	N/A	✔
$\mathcal{H}_\infty$-Analysis	Pirani, Sandberg, and Johansson (2018), Pirani et al. (2015), Pirani, Simpson-Porco, and Fidan (2017)	First-order LTI; Homogeneous	Any	N/A	✔
Frequency-domain analysis	This work	LTI; Heterogeneous	Any	✔	✔

between the performance metrics and the non-zero eigenvalues of the network graph Laplacian, validating the fact that strong network coherence (low $\mathcal{H}_2$-norm) results from the high connectivity of the network (large Laplacian eigenvalues). Unfortunately, the analysis strongly relies on a homogeneity (Andreasson et al., 2017; Bamieh & Gayme, 2013; Bamieh et al., 2012; Oral et al., 2017; Pirani et al., 2017; Tegling et al., 2019) or proportionality (Paganini & Mallada, 2020) assumption of the nodal transfer functions, and thus fails to characterize how individual heterogeneous node dynamics affect the overall coherent network response.

1.1. Our contribution

In this paper, we seek to overcome these limitations by formalizing network coherence through a low-rank structure of the system transfer matrix that appears when the network feedback gain is high. This frequency domain analysis provides a deeper characterization of the role of both network topology and node dynamics on the coherent behavior of the network. In particular, our results make substantial contributions towards the understanding of coordinated and coherent behavior of network systems in many ways:

- **Frequency-domain analysis**: We present a general framework in the frequency domain to analyze the coherence of heterogeneous networks with arbitrary LTI nodal dynamics. We show that network coherence emerges as a low-rank structure of the system transfer matrix as we increase its frequency-dependent algebraic connectivity—a quantity that depends on the network coupling strength and dynamics.
- **Characterization of coherent response**: Our analysis applies to networks with heterogeneous nodal dynamics, and further provides an explicit characterization in the frequency domain of the coherent response to disturbances as the harmonic mean of individual nodal dynamics. Thus, in this way, our results highlight the contribution of individual nodal dynamics to the network's coherent behavior.
- **Time-domain bounds under general inputs**: We formally connect our frequency-domain results with explicit time-domain L_∞ bounds on the difference between individual nodal responses and the coherent dynamic response to a broad class of input signals, suggesting that network coherence is a frequency-dependent phenomenon. That is, the ability of nodes to respond coherently depends on the frequency composition of the input disturbance.
- **Coherent response in large-scale networks**: By providing an exact characterization of the network's coherent dynamics, our analysis can be further applied in settings where only distributional information of the network composition is known. More precisely, we show that the coherent dynamics of tightly connected networks with possibly random nodal dynamics are well approximated by a deterministic transfer function that only depends on the statistical distribution of node dynamics.

Notably, the problem of characterizing coherent dynamic response is unique to heterogeneous networks since the coherent dynamics for homogeneous networks are exactly equal to the common nodal dynamics. In real applications, however, such as power networks, such characterization is relevant to model reduction (Germond, Podmore, 1978) and control design (Jiang, Bernstein, Vorobev, & Mallada, 2021). Our analysis provides, in the asymptotic sense, the exact characterization of coherent dynamics that can be used in control design for heterogeneous networks.

1.2. Comparison with prior work

We compare our work to existing analyses on network coherence (summarized in Table 1):

Slow coherency and Synchrony: Classic coherency analysis (Chow, 1982; Ramaswamy et al., 1996; Romeres et al., 2013; Tyuryukanov et al., 2021) assumes a first- or second-order LTI nodal dynamics, which do not account for more complex dynamics or controllers that are usually present at a node level; e.g., in the power systems literature (Ekomwenrenren et al., 2021; Jiang, Bernstein, et al., 2021; Jiang, Pates, & Mallada, 2021), while our

analyses apply to general LTI nodal dynamics. Moreover, classic analysis lacks theoretical bounds on the difference between the nodal responses and the coherent responses. Our results provide a set of such time-domain bounds (See Section 4).

$\mathcal{H}_2/\mathcal{H}_\infty$-Analyses The seminal paper Bamieh et al. (2012) quantifies network coherence as $\mathcal{H}_2$-norm of the system that maps disturbance to some cohesiveness measure of network states, and Pirani et al. (2018, 2015, 2017) also considered the $\mathcal{H}_\infty$ norm. While $\mathcal{H}_2/\mathcal{H}_\infty$-norm can be computed (Bamieh et al., 2012) for any network with heterogeneous LTI nodes, interpretable closed-form solution can only be obtained when nodal dynamics are homogeneous (Andreasson et al., 2017; Bamieh & Gayme, 2013; Oral et al., 2017; Pirani et al., 2018, 2015, 2017; Tegling et al., 2015, 2019) or proportional to one another (Paganini & Mallada, 2020). More importantly, $\mathcal{H}_2/\mathcal{H}_\infty$-analyses cannot characterize aggregate nodal response. In other words, $\mathcal{H}_2/\mathcal{H}_\infty$-norm only measures how similar nodal responses are close to each other but does not lead to a dynamic representation of the coherent response. On the contrary, our analysis is valid for networks with heterogeneous LTI nodal dynamics and explicitly characterizes the coherent response. Lastly, $\mathcal{H}_2$-analysis implicitly assumes that the network is subjected to white noise disturbance, while our results hold for a broad class of inputs and particularly highlight the role input signals have in the emergence of coherence.

1.3. Other related work

Consensus and synchronization: Consensus (Bamieh et al., 2012; DeGroot, 1974; Ghaedsharaf, Siami, Somarakis, & Motee, 2021; Jadbabaie et al., 2003; Olfati-Saber et al., 2007; Olfati-Saber & Murray, 2004; Tegling et al., 2019) refers to the ability of the network nodes to asymptotically reach a common value over some quantities of interest. Synchronization (Kim, Shim, & Seo, 2011; Mallada, 2014; Mallada et al., 2015; Mirollo & Strogatz, 1990; Nair & Leonard, 2008; Sepulchre et al., 2008; Wieland, Sepulchre, & Allgöwer, 2011) refers to the ability of network nodes to follow a commonly defined trajectory. Although for nonlinear systems synchronization is a structurally stable phenomenon, in the linear case (Kim et al., 2011; Nair & Leonard, 2008; Sepulchre et al., 2008; Wieland et al., 2011), synchronization requires the existence of a common internal model that acts as a virtual leader (Kim et al., 2011; Wieland et al., 2011). As such, consensus and synchronization are coordinated behaviors generally achieved in steady state, and require a common internal model for every node. On the contrary, the network can exhibit coherent behavior during the transient phase (a formal comparison is presented in Section 4.3), and coherence exists even without a common internal model.

Area aggregation and dynamic equivalents: For a group of nodes that exhibit coherent behavior, one can construct dynamic equivalents (Chow, 1982; Ramaswamy et al., 1996) that characterize the slow coherence. Finding the dynamic equivalent, or an aggregate model, for interconnected power generators is a long-standing research subject in power system literature. Previously proposed aggregation model (Anderson & Mirheydar, 1990; Germond, Podmore, 1978; Guggilam, Zhao, Dall'Anese, Chen, & Dhople, 2018; Paganini & Mallada, 2020; Romeres et al., 2013), mostly assume first- or second-order generator dynamics, which does not account for more complex dynamics or controllers (Ekomwenrenren et al., 2021; Jiang, Bernstein, et al., 2021; Jiang, Pates, & Mallada, 2021). Our explicit characterization of coherent dynamics provides a principled way to obtain an aggregate model for general node dynamics.

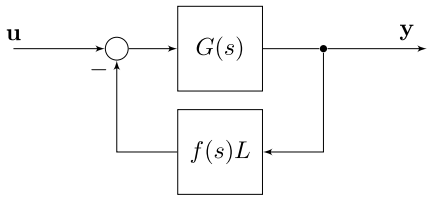

Fig. 1. Block diagram of networked dynamical systems.

1.4. Paper organization

The paper is organized as follows. In Section 3, we discuss the network coherence as a low-rank property of the network transfer matrix. In Section 4, we discuss the time-domain implication of such coherence in the transfer matrix. In Section 5, the dynamics concentration in large-scale networks is discussed. In Section 6, we apply our analysis to synchronous generator networks. Lastly, we conclude with a discussion on future research in Section 7.

Notation. For a vector x, $\|x\| = \sqrt{x^\top x}$ denotes the 2-norm of x, and for a matrix A, $\sigma_{\min}(A)$ denotes the minimum singular value of A, $\|A\|$ denotes the spectral norm of A. Particularly, if A is real symmetric, we let $\lambda_i(A)$ denote the ith smallest eigenvalue of A. We let $\mathrm{diag}\{x_i\}_{i=1}^n$ denote an $n \times n$ diagonal matrix with diagonal entries x_i. We let I_n denote the identity matrix of order n, $\mathbb{1}$ denote column vector $[1, \ldots, 1]^\top$, $[n]$ denote the set $\{1, 2, \ldots, n\}$ and $\mathbb{N}_+$ denote the set of positive integers. We use $\mathbb{S}^{n-1} := \{u \in \mathbb{R}^n : \|u\| = 1\}$ to denote the set of all unit-norm vectors in $\mathbb{R}^n$. Also, we write complex numbers as $a+jb$, where $j = \sqrt{-1}$. We denote $\mathbb{C}$ the field of complex numbers and define the following subsets $\mathcal{B}(s_0, \delta) := \{s \in \mathbb{C} : |s - s_0| \le \delta\}$.

2. Problem setup

Consider a network consisting of n nodes ($n \ge 2$), indexed by $i \in [n]$ with the block diagram structure in Fig. 1. L is the Laplacian matrix of a weighted undirected graph that describes the network interconnection. We further use $f(s)$ to denote the transfer function representing the dynamics of network coupling, and $G(s) = \mathrm{diag}\{g_i(s)\}$ to denote the nodal dynamics, with $g_i(s)$, $i \in [n]$, being a SISO transfer function representing the dynamics of node i. Throughout this paper, we assume all $g_i(s)$, $i = 1, \ldots, n$ and $f(s)$ are rational proper transfer functions, and the Laplacian matrix L is real symmetric.

Under this setting, we can compactly express the transfer matrix from the input signal vector $\mathbf{u}$ to the output signal vector $\mathbf{y}$ by

$$\begin{aligned} T(s) &= (I_n + G(s)f(s)L)^{-1}G(s) \\ &= (I_n + \mathrm{diag}\{g_i(s)\}f(s)L)^{-1}\mathrm{diag}\{g_i(s)\}. \end{aligned} \tag{1}$$

Many existing networks can be represented by this structure. For example, for the first-order consensus network (Olfati-Saber et al., 2007; Olfati-Saber & Murray, 2004), $f(s) = 1$, and the node dynamics are given by $g_i(s) = \frac{1}{s}$. For power networks (Andreasson et al., 2017; Paganini & Mallada, 2020), $f(s) = \frac{1}{s}$, $g_i(s)$ are the dynamics of the generators, and L is the Laplacian matrix representing the sensitivity of power injection w.r.t. bus phase angles. Finally, in transportation networks (Jadbabaie et al., 2003; Olfati-Saber et al., 2007), $g_i(s)$ represent the vehicle dynamics whereas $f(s)L$ describes local inter-vehicle information transfer.

Since L has an eigendecomposition $L = V\Lambda V^\top$ where $V = \left[\frac{\mathbb{1}}{\sqrt{n}}, V_\perp\right]$, $VV^\top = V^\top V = I_n$, and $\Lambda = \text{diag}\{\lambda_i(L)\}$ with $0 = \lambda_1(L) \le \lambda_2(L) \le \cdots \le \lambda_n(L)$, we can rewrite $T(s)$ as

$$\begin{aligned} T(s) &= (I_n + \text{diag}\{g_i(s)\}f(s)L)^{-1}\text{diag}\{g_i(s)\} \\ &= (\text{diag}\{g_i^{-1}(s)\} + f(s)L)^{-1} \\ &= (\text{diag}\{g_i^{-1}(s)\} + f(s)V\Lambda V^\top)^{-1} \\ &= V(V^\top \text{diag}\{g_i^{-1}(s)\}V + f(s)\Lambda)^{-1}V^\top. \end{aligned} \tag{2}$$

As we mentioned in the introduction, we are interested in the regime where the closed-loop system $T(s)$ of (1) has a low-rank structure. To gain some insight, we first consider the following simplified example.

2.1. Simple case: homogeneous network

Suppose $g_i(s)$ are homogeneous, i.e., $g_i(s) = g(s)$. Then using (2) one can decompose $T(s)$ as follows

$$T(s) = \frac{1}{n}g(s)\mathbb{1}\mathbb{1}^\top + V_\perp \text{diag}\left\{\frac{1}{g^{-1}(s) + f(s)\lambda_i(L)}\right\}_{i=2}^{n} V_\perp^\top, \tag{3}$$

where the network dynamics decouple into two terms: 1) the dynamics $\frac{1}{n}g(s)\mathbb{1}\mathbb{1}^\top$ that is independent of network topology and corresponds to the coherent behavior of the system; 2) the remaining dynamics that are dependent on the network structure via both, the eigenvalues $\lambda_i(L), i = 2, \ldots, n$ and the eigenvectors $V_\perp$. Notice that $|f(s)\lambda_2(L)| \le |f(s)\lambda_i(L)|, i = 2, \ldots, n$, then $\frac{1}{n}g(s)\mathbb{1}\mathbb{1}^\top$ is dominant in $T(s)$ as long as $|f(s)\lambda_2(L)|$ (later referred as *frequency-dependent algebraic connectivity*), is large enough to make the norm of the second term in (3) sufficiently small. Following such observation, we can find two regimes where the coherent dynamics $\frac{1}{n}g(s)\mathbb{1}\mathbb{1}^\top$ is dominant:

(1) (*High network connectivity*) If a compact set $S \subset \mathbb{C}$ contains neither zeros nor poles of $g(s)$, then $\lim_{\lambda_2(L)\to\infty} \sup_{s\in S} \left\|T(s) - \frac{1}{n}g(s)\mathbb{1}\mathbb{1}^\top\right\| = 0$.[1]
(2) (*High gain in coupling dynamics*) If s_0 is a pole of $f(s)$, and the network is connected, i.e., $\lambda_2(L) > 0$, then $\lim_{s\to s_0} \left\|T(s) - \frac{1}{n}g(s)\mathbb{1}\mathbb{1}^\top\right\| = 0$.

Such convergence results suggest that if 1) the network has high algebraic connectivity, or 2) our point of interest in the frequency domain is close to a pole of $f(s)$, the response of the entire system is close to one of $\frac{1}{n}g(s)\mathbb{1}\mathbb{1}^\top$. We refer $\frac{1}{n}g(s)\mathbb{1}\mathbb{1}^\top$ as the coherent dynamics[2] in the sense that in such system, the inputs are aggregated, and all nodes have exactly the same response to the aggregate input. *Therefore, coherence of the network corresponds, in the frequency domain, to the property that the network's transfer matrix approximately has a particular rank-one structure.*

The aforementioned analysis can be extended to the case with proportionality assumption, i.e., $g_i(s) = p_i g(s)$ for some $g(s)$ and $p_i > 0, i = 1, \ldots, n$, where one can still obtain decoupled dynamics through proper coordinate transformation (Paganini & Mallada, 2020) and the coherent dynamics are again characterized by the common dynamics $g(s)$. However, it is challenging to analyze the transfer matrix $T(s)$ without the proportionality assumption: First, it is unclear whether a low-rank structure would even emerge under high network connectivity or high gain in the coupling dynamics; Then most importantly, there is no obvious choice for coherent dynamics, hence characterizing the coherent dynamics is a non-trivial problem unique to heterogeneous networks, and no existing work has shown an explicit characterization.

Remark 1. For any connected graph with $\lambda_2(L) > 0$, scaling all the weights by a factor of $\alpha > 1$ leads to a new graph Laplacian αL with $\lambda_2(\alpha L) = \alpha\lambda_2(L)$, thus one can make $\lambda_2(\alpha L)$ arbitrarily large by increasing α, for finite n, and regardless of the network topology. Therefore, high connectivity can be achieved without having a complete graph; However, the motivation behind studying the high connectivity regime is not to achieve some desired level of coherence by increasing the connectivity of the network but rather to provide theoretical explanations for practical networks exhibiting coherent behavior.

2.2. Goal of this work

Our work precisely aims at understanding the coherent dynamics of non-proportional heterogeneous networks. We would like to show that even when $g_i(s)$ are heterogeneous, similar results as in our simple example of homogeneous networks still hold. More precisely, we show that, in Section 3, $T(s)$ converges to a rank-one transfer matrix of the form $\frac{1}{n}\bar{g}(s)\mathbb{1}\mathbb{1}^\top$, as the frequency-dependent algebraic connectivity $|f(s)\lambda_2(L)|$ increases. However, unlike the homogeneous node dynamics case where the coherent behavior is driven by $\bar{g}(s) = g(s)$, the coherent dynamics $\bar{g}(s)$ are given by the harmonic mean of $g_i(s), i = 1, \ldots, n$, i.e.,

$$\bar{g}(s) = \left(\frac{1}{n}\sum_{i=1}^{n} g_i^{-1}(s)\right)^{-1}. \tag{4}$$

The convergence results are presented in the aforementioned two regimes: high network connectivity and high gain in coupling dynamics. We then discuss in Section 4 their implications on the network's time-domain response:

(1) Network with high connectivity responds coherently to a wide class of input signals;
(2) Network with coupling dynamics $f(s) = \frac{1}{s}$ is naturally coherent with respect to sufficiently low-frequency signals, regardless of its connectivity.

One additional feature of our analysis is that it can be further applied in settings where the composition of the network is unknown and only distributional information is present. More precisely, we, in Section 5, consider a network where node dynamics are given by random transfer functions. As the network size grows, the coherent dynamics $\bar{g}(s)$, the harmonic mean of all node dynamics, converge in probability to a deterministic transfer function. We term such a phenomenon, where a family of uncertain large-scale systems concentrates to a common deterministic system, *dynamics concentration*.

Lastly, we verify our theoretical results in Section 6 by several numerical experiments on linearized power network model and discuss a general aggregation model for a group of coherent generators.

3. Coherence in frequency domain

In this section, we analyze the network coherence as the low-rank structure of the transfer matrix in the frequency domain. We start with an important lemma revealing how such coherence is related to the algebraic connectivity $\lambda_2(L)$ and the coupling dynamics $f(s)$.

[1] In this paper, we write most of our convergence results in the high connectivity regime as the limit of differences in norm when $\lambda_2(L) \to \infty$ for simplicity. However, one does not require infinitely high connectivity to achieve coherence. These limits suggest, under sufficiently high connectivity, the transfer matrix $T(s)$ is, in some sense, close to coherent dynamics $\frac{1}{n}g(s)\mathbb{1}\mathbb{1}^\top$. The precise non-asymptotic result is presented in Lemma 2.

[2] We also refer $g(s)$ as the coherent dynamics since transfer matrix of the form $\frac{1}{n}g(s)\mathbb{1}\mathbb{1}^\top$ is uniquely determined by its non-zero eigenvalue $g(s)$.

Lemma 2. *Let $T(s)$ and $\bar{g}(s)$ be defined as in (1) and (4), respectively. Suppose that for $s_0 \in \mathbb{C}$ that is not a pole of $f(s)$, we have*

$$|\bar{g}(s_0)| \leq M_1, \text{ and } \max_{1\leq i\leq n} |g_i^{-1}(s_0)| \leq M_2,$$

for some $M_1, M_2 > 0$. Then the following inequality holds:

$$\left\| T(s_0) - \frac{1}{n}\bar{g}(s_0)\mathbb{1}\mathbb{1}^\top \right\| \leq \frac{(M_1M_2+1)^2}{|f(s_0)|\lambda_2(L) - M_2 - M_1M_2^2}, \tag{5}$$

whenever $|f(s_0)|\lambda_2(L) \geq M_2 + M_1M_2^2$.

We refer readers to Appendix A for the proof. Theorem 4 provides a non-asymptotic bound for our incoherence measure: when $|f(s_0)|\lambda_2$ is sufficiently large, then there exists a constant $C > 0$ such that

$$\left\| T(s_0) - \frac{1}{n}\bar{g}(s_0)\mathbb{1}\mathbb{1}^\top \right\| \leq \frac{CM_1^2M_2^2}{|f(s_0)|\lambda_2(L)}. \tag{6}$$

A large value of $|f(s_0)|\lambda_2(L)$ is sufficient to have the incoherence measure small, and we term this quantity as *frequency-dependent algebraic connectivity*. This term is jointly determined by the algebraic connectivity of the network $\lambda_2(L)$, and the gain of the coupling dynamics $|f(s_0)|$ at the frequency of our interest s_0, which reduces to the standard algebraic connectivity if we evaluate it at some frequency s_0 where $|f(s_0)| = 1$, and gets amplified (or weakened) when $|f(s_0)| > 1$ (or $|f(s_0)| < 1$).

We see that there are two possible ways to achieve such point-wise coherence: Either we increase the network algebraic connectivity $\lambda_2(L)$, by adding edges to the network and increasing edge weights, etc., or we move our point of interest s_0 to a pole of $f(s)$. This point-wise coherence via frequency-dependent connectivity provides the basis of our subsequent analysis. As we mentioned above, we can achieve such coherence by increasing either $\lambda_2(L)$ or $|f(s_0)|$, provided that the other value is fixed and non-zero. Section 3.1 considers the former and Section 3.2 the latter.

3.1. Coherence under high network connectivity

It is intuitive that a network behaves coherently under high connectivity. A formal frequency domain characterization is stated as follows.

Theorem 3. *Let $T(s)$ and $\bar{g}(s)$ be defined as in (1) and (4), respectively. Given a compact set $S \subset \mathbb{C}$, if*

(1) S does not contain any pole of $\bar{g}(s)$;
(2) S does not contain any zero of $g_i(s)$ for $i = 1, \ldots, n$;
(3) $\inf_{s\in S} |f(s)| > 0$,

we have $\lim_{\lambda_2(L)\to+\infty} \sup_{s\in S} \left\| T(s) - \frac{1}{n}\bar{g}(s)\mathbb{1}\mathbb{1}^\top \right\| = 0$.

Proof. On the one hand, since S does not contain any pole of $\bar{g}(s)$, $\bar{g}(s)$ is continuous on the compact set S, and hence bounded (Rudin et al., 1964, Theorem 4.15). On the other hand, because S does not contain any zero of $g_i(s)$, every $g_i^{-1}(s)$ must be continuous on S, and hence bounded as well. It follows that $\max_{1\leq i\leq n} |g_i^{-1}(s)|$ is bounded on S, and the conditions of Lemma 2 are satisfied for all $s \in S$ with a uniform choice of M_1 and M_2. Given any $\lambda_2(L)$ that satisfies $\lambda_2(L) \geq \frac{M_2+M_1M_2^2}{\inf_{s\in S}|f(s)|}$, one can apply (5) for all $s_0 \in S$, which lead to

$$\sup_{s\in S} \left\| T(s) - \frac{1}{n}\bar{g}(s)\mathbb{1}\mathbb{1}^\top \right\| \leq \frac{(M_1M_2+1)^2}{F_l\lambda_2(L) - M_2 - M_1M_2^2},$$

where $F_l = \inf_{s\in S}|f(s)|$. We finish the proof by taking $\lambda_2(L) \to +\infty$ on both sides.

Theorem 3 formally shows that high network connectivity leads to coherence. We emphasize that such coherence is frequency-dependent: the incoherence measure is defined over a compact set S. Roughly speaking, if we would like to see whether the network could have a coherent response under certain input signals, then S should cover most of the frequency components of that signal, as well satisfy the assumptions in Theorem 3. We discuss the proper choice of S when we use Theorem 3 to infer the time-domain response at the beginning of Section 4.

3.2. Coherence under high gain in coupling dynamics

However, high network connectivity is not necessary for coherence. A high gain in the coupling dynamics effectively amplifies the network connection, leading to the following frequency-domain coherence.

Theorem 4. *Let $T(s)$ and $\bar{g}(s)$ be defined as in (1) and (4), respectively. Given a pole of $f(s)$ denoted by s_0, if*

(1) s_0 is not a pole of $\bar{g}(s)$;
(2) s_0 is not a zero of $g_i(s)$ for $i = 1, \ldots, n$,

then $\lim_{s\to s_0} \left\| T(s) - \frac{1}{n}\bar{g}(s)\mathbb{1}\mathbb{1}^\top \right\| = 0$.

Proof. Since s_0 is neither a pole of $\bar{g}(s)$, nor a zero of any $g_i(s)$, $\exists\delta_1 > 0$ such that $\forall s \in \mathcal{B}(s_0, \delta_1)$, we have $|\bar{g}^{-1}(s)| \leq M_1$ and $\max_{1\leq i\leq n} |g_i^{-1}(s)| \leq M_2$ for some $M_1, M_2 > 0$.

Now notice that $\lim_{s\to s_0} |f(s)| = +\infty$, by the definition of the limit, we know that $\exists\delta_2 > 0$ such that $\forall s \in \mathcal{B}(s_0, \delta_2)$, we have $\frac{1}{2}|f(s)|\lambda_2(L) \geq M_2 + M_1M_2^2$. By Lemma 2, let $\delta := \min\{\delta_1, \delta_2\}$, then $\forall s \in \mathcal{B}(s_0, \delta)$, the following holds

$$\begin{aligned} \|T(s) - \frac{1}{n}\bar{g}(s)\mathbb{1}\mathbb{1}^\top\| &\leq \frac{(M_1M_2+1)^2}{|f(s)|\lambda_2(L) - M_2 - M_1M_2^2} \\ &\leq \frac{2\,(M_1M_2+1)^2}{|f(s)|\lambda_2(L)}. \end{aligned}$$

Taking $s \to s_0$, the limit of the right-hand side is 0.

Theorem 4 suggests that for any connected network, some coupling dynamics cause coherent responses from the network under specific input signals. For example, when $f(s) = \frac{1}{s}$, the network $T(s)$ is naturally coherent around $s = 0$, which implies that such a network behaves coherently under sufficiently low-frequency input signals. This is formally justified in Section 4.2, along with time-domain results for other choices of coupling dynamics.

Remark 5. The convergence results presented in this section exclude the region that contains any zero or pole of $\bar{g}(s)$. One can derive convergence results over those regions under certain conditions, but the results is less useful in understanding the network's time-domain behavior. We refer readers to the technical note (Min, Pates, & Mallada, 2021) for details.

4. Implications on time-domain response

In this section, we discuss how one can infer the network's time-domain response using the established frequency-domain coherence in Theorems 3 and 4. Provided that the network $T(s)$ and the coherent dynamics $\bar{g}(s)$ are BIBO stable, we let $\mathbf{y}(t) = [y_1(t), \ldots, y_i(t), \ldots, y_n(t)]^\top$ be the response of the network when the network input is an n-dimensional $U(s)$, and let $\bar{y}(t)$ be the response of $\bar{g}(s)$ to $\frac{\mathbb{1}^\top}{n}U(s)$. The inverse Laplace transform (Dullerud & Paganini, 2013) suggests that for all $i = 1, \ldots, n$, we have

$$|y_i(t) - \bar{y}(t)| = \left| \lim_{\omega\to\infty} \int_{\sigma-j\omega}^{\sigma+j\omega} e^{st} e_i^\top \left(T(s) - \frac{1}{n}\bar{g}(s)\mathbb{1}\mathbb{1}^\top \right) U(s) ds \right|, \tag{7}$$

with a proper choice of $\sigma > 0$. Here e_i is the ith column of identity matrix I_n. This integral can be decomposed into two parts: one integral on the low-frequency band $(\sigma - j\omega_0, \sigma + j\omega_0)$; and another on the high-frequency band $(\sigma - j\infty, \sigma - j\omega_0) \cup (\sigma + j\omega_0, \sigma + j\infty)$, with some choice of ω_0. The former can be shown to be upper bounded by the frequency-domain difference $\|T(s) - \frac{1}{n}\bar{g}(s)\mathbb{1}\mathbb{1}^\top\|$ over the set $S : (\sigma - j\omega_0, \sigma + j\omega_0)$. Then we identify conditions under which this difference is small. In particular,

(1) $\sup_{s\in S} \|T(s) - \frac{1}{n}\bar{g}(s)\mathbb{1}\mathbb{1}^\top\|$ is small under high network connectivity, as suggested by Theorem 3;
(2) $\sup_{s\in S} \|T(s) - \frac{1}{n}\bar{g}(s)\mathbb{1}\mathbb{1}^\top\|$ is small when S is confined in a neighborhood around pole of coupling dynamics $f(s)$, suggested by Theorem 4. The case $f(s) = \frac{1}{s}$ is of the most interest.

Moreover, when $U(s)$ is a sufficiently low-frequency signal such that the high-frequency band $(\sigma - j\infty, \sigma - j\omega_0) \cup (\sigma + j\omega_0, \sigma + j\infty)$ does not include much of its frequency components, the latter integral can be made small. Given an upper bound on the integral in (7), we show that the time-domain response of every node in the network resembles the one from the coherent dynamics $\bar{g}(s)$. Similar to Section 3, we show such time-domain coherence in two regimes: high network connectivity or high gain in the coupling dynamics.

Remark 6. In order to infer the time-domain response, it is necessary that both the transfer functions $T(s)$ and $\frac{1}{n}\bar{g}(s)\mathbb{1}\mathbb{1}^\top$ are stable. Since our primary focus is on the interpretation of the frequency domain results, we are largely working under the tacit assumption that these transfer functions are stable whenever required. It should also be noted that there exists a range of scalable stability criteria in the literature that can be used to guarantee internal stability of the feedback setup in Fig. 1. Perhaps the most well known is that if each $g_i(s)$ is *strictly positive real*, and $f(s)$ is *positive real*, then the transfer functions $\bar{g}(s)$ and $\begin{bmatrix} G(s) \\ I \end{bmatrix} (I + f(s)LG(s))^{-1} \begin{bmatrix} f(s)L & I \end{bmatrix}$ are stable (see e.g. Marquez and Damaren (1995)). Alternative approaches that can be easily adapted to our framework that give criteria that allow for different classes of transfer functions include Jönsson and Kao (2010), Lestas and Vinnicombe (2006), Pates and Mallada (2019).

4.1. Coherent response under high network connectivity

Our first result considers networks with high connectivity.

Theorem 7. *Given a network with node dynamics $\{g_i(s)\}_{i=1}^n$ and coupling dynamics $f(s)$, assume that there exists $\gamma > 0$, such that $\|\bar{g}(s)\|_{\mathcal{H}_\infty} \le \gamma$ and $\|T(s)\|_{\mathcal{H}_\infty} \le \gamma$ for any symmetric Laplacian matrix L. Consider a network coupling $f(s)$ and a real input signal vector $\mathbf{u}(t)$ with its Laplace transform $U(s)$ such that for some $\sigma \ge 0$, we have*

(1) $\inf_{\omega\in\mathbb{R}} |f(\sigma + i\omega)| > 0$;
(2) $\sup_{Re(s)>\sigma} \|U(s)\|$ *is finite;*
(3) $\lim_{\omega\to\infty} \int_{\sigma+j0}^{\sigma+j\omega} \|U(s)\| ds$ *is finite.*

The following holds:

- *If $\sigma = 0$, then for any $\epsilon > 0$, there exists a $\lambda > 0$, such that whenever $\lambda_2(L) \ge \lambda$, we have $\|\mathbf{y}(t) - \bar{y}(t)\mathbb{1}\|_{\mathcal{L}_\infty} \le \epsilon$, i.e.,*

$$\max_{i\in[n]} \sup_{t>0} |y_i(t) - \bar{y}(t)| \le \epsilon.$$

- *If $\sigma > 0$, then given any $\epsilon > 0$ and $T > 0$, there exists a $\lambda > 0$, such that whenever $\lambda_2(L) \ge \lambda$, we have*

$$\max_{i\in[n]} \sup_{0<t<T} |y_i(t) - \bar{y}(t)| \le \epsilon.$$

We refer readers to Appendix B for the proof. Theorem 7 provides a formal explanation of coherent behavior observed in practical networks and shows its relation with network connectivity. That is, a stable network with high connectivity can respond coherently to a class of input signals. More importantly, the coherent response is well approximated by $\bar{g}(s)$; hence, it suffices to study $\bar{g}(s)$ to understand the coherent behavior of a network with high connectivity.

Furthermore, depending on the poles of the signal $U(s)$, our results vary: When $U(s)$ has no pole on the imaginary axis (exponentially decaying signals), our time-domain bounds between system response $\mathbf{y}(t)$ and the coherent response $\bar{y}(t)\mathbb{1}$ holds notably for all time $t > 0$. When $U(s)$ has poles on the imaginary axis, our theoretical analysis only provides the time-domain bound within some time interval $[0, T]$, due to some limitations in our current proof techniques. Refining the bound for the latter scenario is left for future research.

While the theorem suggests that some level of coherence can be achieved by increasing the network connectivity, one should be cautious about the potential network instability caused by strong interconnection. Nonetheless, some simple passivity-motivated criteria that ensure stability even as $\lambda_2(L)$ becomes arbitrarily large:

Theorem 8. *Suppose that all $g_i(s)$, $i = 1, \dots, n$ are* output strictly passive*: $Re(g_i(s)) \ge \epsilon |g_i(s)|^2$, $\forall Re(s) > 0$, for some $\epsilon > 0$, and $f(s)$ is* positive real*: $Re(f(s)) \ge 0$, $\forall Re(s) > 0$, then there exists $\gamma > 0$, such that given any positive semidefinite matrix L, we have*

$$\|\bar{g}(s)\|_{\mathcal{H}_\infty} \le \gamma, \text{ and } \|T(s)\|_{\mathcal{H}_\infty} \le \gamma.$$

We refer readers to the technical note (Min et al., 2021) for the proof. Theorem 8, together with Theorem 7, shows that for certain passive networks, the coherence can be achieved over a class of input signals by increasing the network connectivity.

Remark 9. Besides network stability as a prerequisite, a few assumptions are made in Theorem 7: infimum on $|f(s)|$ ensures that the network coupling does not vanish over our domain of interest; supremum on $\|U(s)\|$ is needed for utilizing inverse Laplace transform; and the last assumption requires $U(s)$ to have a light tail on the high-frequency range. A low-frequency signal with no abrupt change at $t = 0$ satisfies the assumption with some $\sigma > 0$, for example, sinusoidal signal $U(s) = \frac{\alpha}{s^2+\alpha^2}\mathbf{u}_0$, or exponential approach signal $U(s) = \frac{\alpha}{s(s+\alpha)}\mathbf{u}_0$ of some shape $\mathbf{u}_0 \in \mathbb{R}^n$. Moreover, if one adds an exponential decay to the aforementioned input signal, then the new signal $U(s - \nu)$ ($\nu > 0$ can be arbitrarily small) satisfies the assumption with $\sigma = 0$.

4.2. Coherent response under special coupling dynamics

As we discussed in Section 3, coherence is not all about network connectivity, and high gain in the coupling dynamics causes coherence as well. One simple and practically seen coupling dynamics are $f(s) = \frac{1}{s}$. Due to its high gain at $s = 0$, we expect that the network has a coherent response under low-frequency signals, as formally shown below.

Theorem 10. *Given a network with node dynamics $\{g_i(s)\}_{i=1}^n$, coupling dynamics $f(s) = \frac{1}{s}$, and a fixed graph Laplacian L with $\lambda_2(L) > 0$, such that $\|\bar{g}(s)\|_{\mathcal{H}_\infty}$ and $\|T(s)\|_{\mathcal{H}_\infty}$ are finite. Then for*

any $\epsilon > 0$ and $T > 0$, there exists an $\alpha_0 > 0$ such that if the network input is either (we use $\chi(t) = \mathbf{1}_{t\geq 0}$ to denote step signal)

- *a sinusoidal signal $\mathbf{u}_\alpha(t) = \sin(\alpha t)\chi(t)\mathbf{u}_0$ with $0 \leq \alpha \leq \alpha_0$, in an arbitrary direction $\mathbf{u}_0 \in \mathbb{S}^{n-1}$;*
- *or a general input $\mathbf{u}(t) = \sum_{j=1}^{\infty} \beta_j \sin(\alpha_j t)\chi(t)\mathbf{u}_j$, with $\mathbf{u}_j \in \mathbb{S}^{n-1}$, $0 \leq \alpha_j \leq \alpha_0$, $\beta_j \geq 0$, $\forall j = 1, \ldots$, and $\sum_{j=1}^{\infty} \beta_j \leq 1$,*

we have $\max_{i\in[n]} \sup_{0<t<T} |y_i(t) - \bar{y}(t)| \leq \epsilon$

We refer readers to Appendix B for the proof. Theorem 10 shows that a stable network with $f(s) = \frac{1}{s}$ is naturally coherent subject to sufficiently low-frequency signals, regardless of its connectivity. Notably, the requirement on the node dynamics here is much weaker than one in Theorem 7 as we only need to establish stability for a given interconnection L, whereas Theorem 7 requires stability under any interconnection. However, similar to Theorem 7 applying to signals with poles on the imaginary axis, our results only provide the bound in the transient phase until some time $T > 0$. We believe it is possible to provide an error bound for all time $t > 0$ if an exponential decay is added to the sinusoidal inputs, similar to the result in Theorem 7 for the case of $\sigma = 0$, and a formal proof is left to future research.

4.3. Comparison with different notions of coordination

Our Theorems 7 and 10 show the coherent response of the network in the time domain. We compare our results to prior work that studies different forms of time-domain coordination in network systems.

The consensus (Olfati-Saber & Murray, 2004) and synchronization (Mallada et al., 2015; Mirollo & Strogatz, 1990; Sepulchre et al., 2008) are arguably the simplest form of coordination in network systems, which can be viewed as a problem tracking some reference signal $\bar{y}(t)$ representing the final consensus or synchronization. However, one only requires $y_i(t) \to \bar{y}(t)$ when $t \to \infty$, i.e., that the node responses become close to $\bar{y}(t)$ in steady state. The coherent response considered here is different in that we have $y_i(t) \simeq \bar{y}(t)$, $\forall t > 0$, i.e., $\bar{y}(t)$ is a good approximation for $y_i(t)$ for all time $t > 0$, hence our results can be also used for transient analysis.

The work on coherency and synchrony (Ramaswamy et al., 1996; Ramaswamy, Verghese, Rouco, Vialas, & DeMarco, 1995; Sastry & Varaiya, 1981; Wu & Narasimhamurthi, 1983) studies a similar behavior as ours, but the behavior is characterized as pairwise coherence achieved under input signal of certain spatial shape: given an input signal vector $\mathbf{u}(t) = v(t)\mathbf{u}_0$, Ramaswamy et al. (1995), Wu and Narasimhamurthi (1983) shows the condition on $\mathbf{u}_0$ such that the responses of some pair of nodes are similar (or generally, proportional (Ramaswamy et al., 1996)), i.e., $y_i(t) \simeq y_j(t)$ for some $i, j \in [n]$. Our results show that certain temporal shape $v(t)$ also causes coherence, and in a stronger form: our coherence does not depend on the shape u_0 and holds for all nodes.

5. Dynamics concentration in large-scale networks

In Section 3, we looked into convergence results of $T(s)$ for networks with fixed size n. However, one could easily see that such coherence depends mildly on the network size n: In Lemma 2, as long as the bounds regarding $g_i(s)$, i.e. M_1 and M_2 do not scale with respect to n, coherence can emerge as the network size increases. This is the topic of this section.

5.1. Coherence in large-scale networks

To start with, we revise the problem settings to account for variable network size: Let $\{g_i(s), i \in \mathbb{N}_+\}$ be a sequence of transfer functions, and $\{L_n, n \in \mathbb{N}_+\}$ be a sequence of real symmetric Laplacian matrices such that L_n is a square matrix of order n, particularly, let $L_1 = 0$. Then we define a sequence of transfer matrix $T_n(s)$ as

$$T_n(s) = (I_n + G_n(s)L_n)^{-1} G_n(s), \tag{8}$$

where $G_n(s) = \text{diag}\{g_1(s), \ldots, g_n(s)\}$. This is exactly the same transfer matrix shown in Fig. 1 for a network of size n. We can then define the coherent dynamics for every $T_n(s)$ as $\bar{g}_n(s) = \left(\frac{1}{n}\sum_{i=1}^{n} g_i^{-1}(s)\right)^{-1}$.

For certain family $\{L_n, n \in \mathbb{N}_+\}$ of large-scale networks, the network algebraic connectivity $\lambda_2(L_n)$ increases as n grows. For example, when L_n is the Laplacian of a complete graph of size n with all edge weights being 1, we have $\lambda_2(L_n) = n$. As a result, network coherence naturally emerges as the network size grows. Recall that to prove the convergence of $T_n(s)$ to $\frac{1}{n}\bar{g}_n(s)\mathbb{1}\mathbb{1}^\top$ for fixed n, we essentially seek for $M_1, M_2 > 0$, such that $|\bar{g}_n(s)| \leq M_1$ and $\max_{1\leq i\leq n} |g_i^{-1}(s)| \leq M_2$ for s in a certain set. If it is possible to find a universal $M_1, M_2 > 0$ for all n, then the convergence results should be extended to arbitrarily large networks, provided that network connectivity increases as n grows. The results follow after we state the notion of uniform boundedness for a family of functions.

Definition 11. Let $\{g_i(s), i \in \mathcal{I}\}$ be a family of complex functions indexed by $\mathcal{I}$. Given $S \subset \mathbb{C}$, $\{g_i(s), i \in \mathcal{I}\}$ is uniformly bounded on S if

$$\exists M > 0 \quad s.t. \quad |g_i(s)| \leq M, \quad \forall i \in \mathcal{I}, \ \forall s \in S.$$

Theorem 12. *Suppose $\lambda_2(L_n) \to +\infty$ as $n \to \infty$. Given a compact set $S \subset \mathbb{C}$, if both $\{g_i^{-1}(s), i \in \mathbb{N}_+\}$ and $\{\bar{g}_n(s), n \in \mathbb{N}_+\}$ are uniformly bounded on a set $S \subset \mathbb{C}$, and $\inf_{s\in S}|f(s)| > 0$, then we have*

$$\lim_{n\to\infty} \sup_{s\in S} \left\| T_n(s) - \frac{1}{n}\bar{g}_n(s)\mathbb{1}\mathbb{1}^\top \right\| = 0.$$

The proof is similar to the one for Theorem 3. Due to space constraints, we refer readers to the technical note (Min et al., 2021) for the proof. Interestingly, in a stochastic setting where all $g_i(s)$ are unknown transfer functions independently drawn from some distribution, their harmonic mean $\bar{g}_n(s)$ eventually converges in probability to a deterministic transfer function as the network size increases. Consequently, a large-scale network consisting of random node dynamics (to be formally defined later) concentrates around a deterministic system. We term this phenomenon *dynamics concentration*.

Remark 13. In this section, we only discuss the coherence due to connectivity since the coherence from a high gain in coupling dynamics shown in Theorem 4 can be applied to any connected network, regardless of its size.

5.2. Dynamics concentration in large-scale networks

Now we consider the cases where the node dynamics are unknown (stochastic). For simplicity, we constraint our analysis to the setting where the node dynamics are independently sampled from the same random rational transfer function with all or part of the coefficients are random variables, i.e. the nodal transfer functions are of the form

$$g_i(s) \sim \frac{b_m s^m + \cdots b_1 s + b_0}{a_l s^l + \cdots a_1 s + a_0}, \tag{9}$$

for some $m, l > 0$, where $b_0, \ldots, b_m$, $a_0, \ldots, a_l$ are random variables.

To formalize the setting, we first define the random transfer function to be sampled. Let $\Omega = \mathbb{R}^d$ be the sample space, $\mathcal{F}$ the

Borel σ-field of Ω, and $\mathbb{P}$ a probability measure on Ω. A sample $w \in \Omega$ thus represents a d-dimensional vector of coefficients. We then define a random rational transfer function $g(s, w)$ on $(\Omega, \mathcal{F}, \mathbb{P})$ such that all or part of the coefficients of $g(s, w)$ are random variables. Then for any $w_0 \in \Omega$, $g(s, w_0)$ is a rational transfer function.

Now consider the probability space $(\Omega^\infty, \mathcal{F}^\infty, \mathbb{P}^\infty)$. Every $\mathbf{w} \in \Omega^\infty$ gives an instance of samples drawn from our random transfer function:

$$g_i(s, w_i) := g(s, w_i), i \in \mathbb{N}_+,$$

where w_i is the ith element of $\mathbf{w}$. By construction, $g_i(s, w_i), i \in \mathbb{N}_+$ are i.i.d. random transfer functions. Moreover, for every $s_0 \in \mathbb{C}$, $g_i(s_0, w_i), i \in \mathbb{N}_+$ are i.i.d. random complex variables taking values in the extended complex plane (presumably taking value ∞).

Now given $\{L_n, n \in \mathbb{N}_+\}$ a sequence of $n \times n$ real symmetric Laplacian matrices, consider the random network of size n whose nodes are associated with the dynamics $g_i(s, w_i), i = 1, 2, \ldots, n$ and coupled through L_n. The transfer matrix of such a network is given by

$$T_n(s, \mathbf{w}) = (I_n + G_n(s, \mathbf{w})L_n)^{-1}G_n(s, \mathbf{w}), \tag{10}$$

where $G_n(s, \mathbf{w}) = \text{diag}\{g_1(s, w_1), \ldots, g_n(s, w_n)\}$. Then under this setting, the coherent dynamics of the network are given by

$$\bar{g}(s, \mathbf{w}) = \left(\frac{1}{n}\sum_{i=1}^{n} g_i^{-1}(s, w_i)\right)^{-1}. \tag{11}$$

Now given a compact set $S \subset \mathbb{C}$ of interest, and assuming suitable conditions on the distribution of $g(s, w)$, we expect that the random coherent dynamics $\bar{g}(s, \mathbf{w})$ would converge uniformly in probability to its expectation

$$\hat{g}(s) = \left(\mathbb{E}g^{-1}(s, w)\right)^{-1} := \left(\int_\Omega g^{-1}(s, w)d\mathbb{P}(w)\right)^{-1}, \tag{12}$$

for all $s \in S$, as $n \to \infty$. The following Lemma provides a sufficient condition for this to hold.

Lemma 14. *Consider the probability space $(\Omega^\infty, \mathcal{F}^\infty, \mathbb{P}^\infty)$. Let $\bar{g}_n(s, \mathbf{w})$ and $\hat{g}(s)$ be defined as in (11) and (12), respectively, and given a compact set $S \subset \mathbb{C}$, let the following conditions hold:*

(1) $g^{-1}(s, w)$ is uniformly bounded on $S \times \Omega$;
(2) $\{\bar{g}_n(s, \mathbf{w}), n \in \mathbb{N}_+\}$ are uniformly bounded on $S \times \Omega^\infty$;
(3) $\exists C_{lip} > 0$ s.t. $|g_i^{-1}(s_1, w) - g_i^{-1}(s_2, w)| \le C_{lip}|s_1 - s_2|$, $\forall w \in \Omega$, $\forall s_1, s_2 \in S$, $\forall i$;
(4) $\hat{g}(s)$ is uniformly continuous on S.

Then, $\forall \epsilon > 0$, we have

$$\lim_{n\to\infty} \mathbb{P}\left(\sup_{s\in S}\left\|\frac{1}{n}\bar{g}_n(s, \mathbf{w})\mathbb{1}\mathbb{1}^\top - \frac{1}{n}\hat{g}(s)\mathbb{1}\mathbb{1}^\top\right\| \ge \epsilon\right) = 0.$$

This lemma suggests that our coherent dynamics $\bar{g}_n(s, \mathbf{w})$, as n increases, converges uniformly on S to its expected version $\hat{g}(s)$. Then provided that the coherence is obtained as the network size grows, we would expect that the random transfer matrix $T_n(s, \mathbf{w})$ to concentrate to a deterministic one $\frac{1}{n}\hat{g}(s)\mathbb{1}\mathbb{1}^\top$, as the following theorem shows.

Theorem 15. *Given probability space $(\Omega^\infty, \mathcal{F}^\infty, \mathbb{P}^\infty)$. Let $T_n(s, \mathbf{w})$ and $\hat{g}(s)$ be defined as in (10) and (12), respectively. Suppose $\lambda_2(L_n) \to +\infty$ as $n \to +\infty$. Given a compact set $S \subset \mathbb{C}$, if all the conditions in Lemma 14 hold, then $\forall \epsilon > 0$, we have*

$$\lim_{n\to\infty} \mathbb{P}\left(\sup_{s\in S}\left\|T_n(s, \mathbf{w}) - \frac{1}{n}\hat{g}(s)\mathbb{1}\mathbb{1}^\top\right\| \ge \epsilon\right) = 0.$$

The proof of Lemma 14 follows the standard procedure for showing the uniform stochastic convergence of a random function, then Theorem 15 is its direct application. We refer interested readers to the technical note (Min et al., 2021) for the proofs. In summary, because the coherent dynamics is given by the harmonic mean of all node dynamics $g_i(s)$, it concentrates around its harmonic expectation $\hat{g}(s)$ as the network size grows. As a result, in practice, the coherent behavior of large-scale networks depends on the empirical distribution of $g_i(s)$, i.e. a collective effect of all node dynamics rather than every individual node dynamics. For example, two different realizations of large-scale networks with dynamics $T_n(s, \mathbf{w})$ exhibit similar coherent behavior with high probability, in spite of the possible substantial differences in individual node dynamics.

Remark 16. With Theorem 15, one can adopt the analysis in Section 4 to derive a time-domain result similar to the one in Theorem 7. In this case, the network stability again relies on node passivity as required in Theorem 8. Nonetheless, for the low-order rational transfer function, the condition of being passive is equivalent to its coefficients satisfying certain algebraic inequalities (Chen & Smith, 2009); hence there exists probability measure $\mathbb{P}$ on the coefficients such that the resulting transfer function is passive almost surely, under which the time-domain response of the network $T_n(s, \mathbf{w})$ can be inferred.

6. Application: Aggregate dynamics of synchronous generator networks

In this section, we apply our analysis to investigate coherence in power networks. For coherent generator groups, we find that $\frac{1}{n}\bar{g}(s)$ generalizes typical aggregate generator models, which are often used for model reduction in power networks (Chow, 2013). Moreover, we show that heterogeneity in generator dynamics usually leads to high-order aggregate dynamics, making it challenging to find a reasonably low-order approximation. Consider the transfer matrix of power generator networks (Paganini & Mallada, 2020) linearized around its steady-state point, given by the following block diagram (see Fig. 3). This is exactly the block structure shown in Fig. 1 with $f(s) = \frac{1}{s}$. Here, the network output, i.e., the frequency deviation of each generator, is denoted by ω. Generally, the $g_i(s)$ are modeled as strictly positive real transfer functions, and we assume L is connected. Such interconnection is stable (Marquez & Damaren, 1995), regardless of the network connectivity.

6.1. Numerical verification

We verify our theoretical results, Theorems 7 and 10, with numerical simulations on the Icelandic power grid (University of Edinburgh, 2003). Specifically, the generator models are either modeled as a first-order $g_i(s) = \frac{1}{m_i s + d_i}$ or a second-order $g_i(s) = \frac{\tau_i s + 1}{(\tau_i s + 1)(m_i s + d_i) + r_i^{-1}}$. The order of the generator model and the coefficients are all provided in University of Edinburgh (2003), except for damping ratio d_i, which we set to $\frac{1}{2\pi\omega_0}$ times the rating of the ith generator (ω_0 is the nominal frequency 60 Hz). The Laplacian L is given by $L_{ij} = \frac{\partial}{\partial\theta_j}\sum_{k=1}^{n}|V_i||V_k|b_{ik}\sin(\theta_i - \theta_k)\Big|_{\theta=\theta_0}$, where θ_0 are angle deviations at steady state, $|V_i|$ is the voltage magnitude at bus i and b_{ij} is the line susceptance. All these line/bus information is available in University of Edinburgh (2003).

The connectivity L_{ij} between two generator buses (nodes) critically, and inversely, depends on their physical distance (longer transmission line means smaller b_{ij}, the line susceptance). Since the Icelandic power grid has all its generator buses relatively

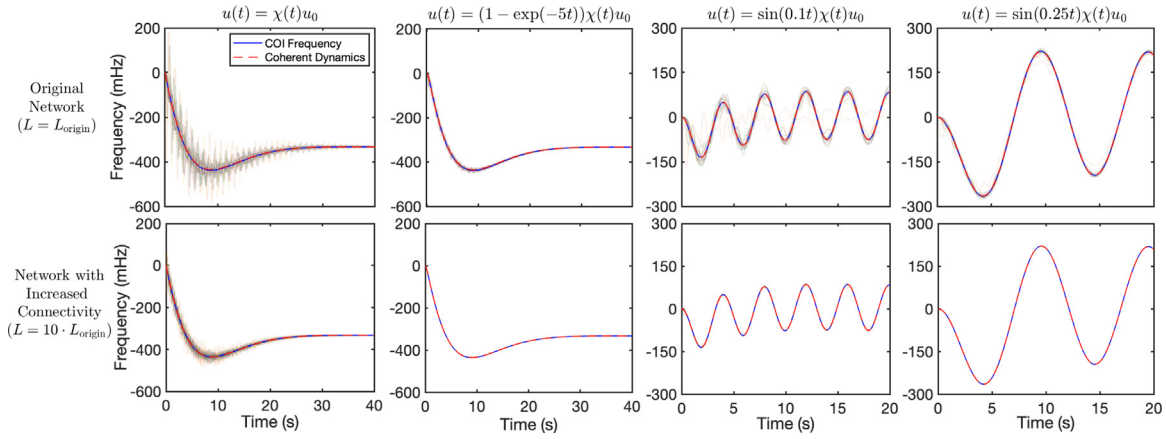

Fig. 2. Coherent response of Icelandic Grid. Each column corresponds to a different input signal (from left to right: step, exponential approach, high-frequency sinusoidal, and low-frequency sinusoidal signal. Here we use $\chi(t) = \mathbf{1}_{t\geq 0}$ to denote step signal); The input signal has a shape $u_0 = -e_2$, i.e., only the second node is subject to disturbance. The top row shows the responses of the original Icelandic grid, and the bottom row shows the responses of the network with increased connectivity. The red dashed line shows the response of $\bar{g}(s)$ subject to the averaged input $\bar{u}(t) = \mathbb{1}^\top u(t)/n$. Blue solid line shows the Center-of-Inertia frequency of the grid $y_{\text{COI}} = (\sum_{i=1}^n m_i y_i)/(\sum_{i=1}^n m_i)$.

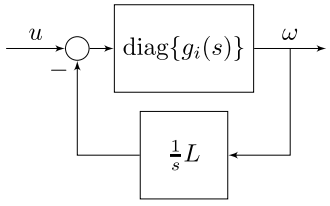

Fig. 3. Block Diagram of Linearized Power Networks.

close to each other, the grid naturally has sufficiently high connectivity to exhibit coherent behavior, as we will verify now. We plot in Fig. 2 the frequency response of the power network model subject to various input disturbances. The network step response is already highly coherent, i.e. response of every single node (generator) is close to the one of the coherent dynamics $\bar{g}(s)$, in the original network and even more coherent when the network connectivity is scaled up, as suggested by Theorem 7. We note that scaling up the network Laplacian means bringing generators closer geographically, which is generally unrealistic. We do so mostly for illustration purposes, highlighting how the level of network coherence depends on connectivity. In addition, the network responds more coherently when subject to lower-frequency signals (See the second and fourth column in Fig. 2), as suggested by Theorem 10. But most importantly, the coherent dynamics $\bar{g}(s)$ provides a good characterization of the coherent response. We also plot the Center-of-Inertia frequency of the grid $y_{\text{COI}} = (\sum_{i=1}^n m_i y_i)/(\sum_{i=1}^n m_i)$, which is generally used for frequency response assessment, and we see that it is well approximated by the response of $\bar{g}(s)$.

6.2. Aggregate dynamics of generator networks

The numerical simulations above suggest that the coherent dynamics $\bar{g}(s)$ characterize well the overall frequency response of generators in a grid. This leads to a general methodology to analyze the aggregate dynamics of such networks. Let

$$g_{\text{aggr}}(s) := \frac{1}{n}\bar{g}(s) = \left(\sum_{i=1}^n g_i^{-1}(s)\right)^{-1}.$$

Our analysis suggests that the transfer function $T(s)$ representing a network of generators is close $g_{\text{aggr}}(s)\mathbb{1}\mathbb{1}^\top$ within the low-frequency range, for sufficiently high network connectivity $\lambda_2(L)$. We can also view $g_{\text{aggr}}(s)$ as the aggregate generator dynamics, in the sense that it takes the sum of disturbances $\mathbb{1}^\top u = \sum_{i=1}^n u_i$ as its input, and its output represents the coherent response of all generators.

Such a notion of aggregate dynamics is important in modeling large-scale power networks (Chow, 2013). Generally speaking, one seeks to find an aggregate dynamic model for a group of generators using the same structure (transfer function) as individual generator dynamics, i.e. when generator dynamics are modeled as $g_i(s) = g(s;\theta_i)$, where θ_i is a vector of parameters representing physical properties of each generator, existing works (Germond, Podmore, 1978; Guggilam et al., 2018) propose methods to find aggregate dynamics of the form $g(s;\theta_{\text{aggr}})$ for certain structures of $g(s;\theta)$. Our $g_{\text{aggr}}(s)$ justifies their choices of θ_{aggr}, as shown in the following example.

Example 17. For generators given by the swing model $g_i(s) = \frac{1}{m_i s + d_i}$, where m_i, d_i are the inertia and damping of generator i, respectively. The aggregate dynamics are

$$g_{\text{aggr}}(s) = \frac{1}{m_{\text{aggr}} s + d_{\text{aggr}}}, \tag{13}$$

where $m_{\text{aggr}} = \sum_{i=1}^n m_i$ and $d_{\text{aggr}} = \sum_{i=1}^n d_i$.

Here the parameters are $\theta = \{m, d\}$. The aggregate model given by (13) is consistent with the existing approach of choosing inertia m and damping d as the respective sums over all the coherent generators.

However, as we show in the next example when one considers more involved models, it is challenging to find parameters that accurately fit the aggregate dynamics.

Example 18. For generators given by the swing model with turbine droop $g_i(s) = \frac{1}{m_i s + d_i + \frac{r_i^{-1}}{\tau_i s + 1}}$, where r_i^{-1} and τ_i are the droop coefficient and turbine time constant of generator i, respectively. The aggregate dynamics are given by

$$g_{\text{aggr}}(s) = \frac{1}{m_{\text{aggr}} s + d_{\text{aggr}} + \sum_{i=1}^n \frac{r_i^{-1}}{\tau_i s + 1}}. \tag{14}$$

Here the parameters are $\theta = \{m, d, r^{-1}, \tau\}$. This example illustrates, in particular, the difficulty in aggregating generators with heterogeneous turbine time constants. If the τ_i are heterogeneous, then $g_{\text{aggr}}(s)$ is a high-order transfer function and

cannot be accurately represented by a single generator model parametrized by θ. The aggregation of generators essentially asks for a low-order approximation of $g_{\text{aggr}}(s)$. Our analysis reveals the fundamental limitation of using conventional approaches seeking aggregate dynamics with the same structure of individual generators. Furthermore, by characterizing the aggregate dynamics in the explicit form $g_{\text{aggr}}(s)$, one can develop more accurate low-order approximation (Min & Mallada, 2021). Lastly, we emphasize that our analysis does not depend on a specific model of generator dynamics $g_i(s)$. Hence, it provides a general methodology to aggregate coherent generator networks.

7. Conclusions

In this paper, we study network coherence as a low-rank property of the transfer matrix $T(s)$ in the frequency domain. The analysis leads to useful characterizations of coordinated behavior and justifies the relation between network coherence and network frequency-dependent algebraic connectivity. Our results suggest that network coherence is a frequency-dependent phenomenon, which is numerically illustrated in generator networks. Lastly, concentration results for large-scale networks are presented, revealing the exclusive role of the statistical distribution of node dynamics in determining the coherent dynamics of such networks. One interesting future work is to study the dynamic behavior of large-scale networks with multiple coherent groups. One could model the inter-community interactions by replacing the dynamics of each community with its coherent one, or more generally, a reduced one. Although clustering, i.e. finding communities, for homogeneous networks can be efficiently done by various graph-based methods, it is still open for research to find multiple coherent groups in heterogeneous dynamical networks.

Acknowledgments

This work was done by H. Min during his Ph.D. study at Johns Hopkins University. H. Min and E. Mallada acknowledge the support from the U.S. National Science Foundation through grant Global Center 90107717 and Johns Hopkins University IAA Grant Challenge. R. Pates acknowledges the funding from the ELLIIT Strategic Research Area, ERC grant agreement No 834142, and the initiative COMPEL with funding from the Swedish government. A preliminary version of this work, covering an alternative version of the results in Section 5, was presented in Min and Mallada (2019).

Appendix A. Proof of Lemma 2

Proof. Let $H = V^\top \text{diag}\{g_i^{-1}(s_0)\}V + f(s_0)\Lambda$, such that (2) becomes $T(s) = VH^{-1}V^\top$. Then it is easy to see that

$$\begin{aligned}\|T(s_0) - \frac{1}{n}\bar{g}(s_0)\mathbb{1}\mathbb{1}^\top\| &= \|T(s_0) - \bar{g}(s_0)Ve_1e_1^\top V^\top\| \\ &= \|V\left(H^{-1} - \bar{g}(s_0)e_1e_1^\top\right)V^\top\| \\ &= \|H^{-1} - \bar{g}(s_0)e_1e_1^\top\|, \end{aligned} \tag{A.1}$$

where e_1 is the first column of identity matrix I_n. The first equality holds by noticing that $\frac{\mathbb{1}}{\sqrt{n}}$ is the first column of V.

With $V = \begin{bmatrix}\frac{\mathbb{1}}{\sqrt{n}} & V_\perp\end{bmatrix}$, we write H in block matrix form:

$$\begin{aligned} H &= \begin{bmatrix}\frac{\mathbb{1}^\top}{\sqrt{n}} \\ V_\perp^\top\end{bmatrix}\text{diag}\{g_i^{-1}(s_0)\}\begin{bmatrix}\frac{\mathbb{1}}{\sqrt{n}} & V_\perp\end{bmatrix} + f(s_0)\Lambda \\ &:= \begin{bmatrix}\bar{g}^{-1}(s_0) & h_{21}^\top \\ h_{21} & H_{22}\end{bmatrix},\end{aligned}$$

where

$$\begin{aligned} h_{21} &= V_\perp^\top \text{diag}\{g_i^{-1}(s_0)\}\frac{\mathbb{1}}{\sqrt{n}}, \\ H_{22} &= V_\perp^\top \text{diag}\{g_i^{-1}(s_0)\}V_\perp + f(s_0)\tilde{\Lambda}, \\ \tilde{\Lambda} &= \text{diag}\{\lambda_2(L), \dots, \lambda_n(L)\}. \end{aligned}$$

Inverting H in its block form, we have

$$H^{-1} = \begin{bmatrix} a & -ah_{21}^\top H_{22}^{-1} \\ -aH_{22}^{-1}h_{21} & H_{22}^{-1} + aH_{22}^{-1}h_{21}h_{21}^\top H_{22}^{-1}\end{bmatrix},$$

where $a = \frac{1}{\bar{g}^{-1}(s_0) - h_{21}^\top H_{22}^{-1}h_{21}}$.

By our assumption, we have $\|\text{diag}\{g_i^{-1}(s_0)\}\| = \max_{1\le i\le n}|g_i^{-1}(s_0)| \le M_2$, then

$$\begin{aligned}\|h_{21}\| &= \|V_\perp^\top \text{diag}\{g_i^{-1}(s_0)\}\frac{\mathbb{1}}{\sqrt{n}}\| \\ &\le \|V_\perp\|\|\text{diag}\{g_i^{-1}(s_0)\}\|\frac{\|\mathbb{1}\|}{\sqrt{n}} \le M_2, \end{aligned} \tag{A.2}$$

and

$$\begin{aligned}\|H_{22}^{-1}\| &= \|(f(s_0)\tilde{\Lambda} + V_\perp^\top \text{diag}\{g_i^{-1}(s_0)\}V_\perp)^{-1}\| \\ &= \frac{1}{\sigma_{\min}\left(f(s_0)\tilde{\Lambda} + V_\perp^\top \text{diag}\{g_i^{-1}(s_0)\}V_\perp\right)} \\ &\le \frac{1}{\sigma_{\min}(f(s_0)\tilde{\Lambda}) - \|V_\perp^\top \text{diag}\{g_i^{-1}(s_0)\}V_\perp\|} \\ &\le \frac{1}{\sigma_{\min}(f(s_0)\tilde{\Lambda}) - M_2} \le \frac{1}{|f(s_0)|\lambda_2(L) - M_2}, \end{aligned} \tag{A.3}$$

whenever $|f(s_0)|\lambda_2(L) > M_2$.

Lastly, when $|f(s_0)|\lambda_2(L) > M_2 + M_2^2M_1$, a similar reasoning as above, using (A.2) (A.3), and our assumption $|\bar{g}(s_0)| \le M_1$, gives

$$\begin{aligned}|a| &\le \frac{1}{|\bar{g}^{-1}(s_0)| - \|h_{21}\|^2\|H_{22}^{-1}\|} \\ &= \frac{(|f(s_0)|\lambda_2(L) - M_2)M_1}{|f(s_0)|\lambda_2(L) - M_2 - M_1M_2^2}. \end{aligned} \tag{A.4}$$

Now we bound the norm of $H^{-1} - \bar{g}(s_0)e_1e_1^\top$ by the sum of norms of all its blocks:

$$\begin{aligned}&\|H^{-1} - \bar{g}(s_0)e_1e_1^\top\| \\ &\le |a\bar{g}(s_0)h_{21}^\top H_{22}^{-1}h_{21}| + 2\|aH_{22}^{-1}h_{21}\| \\ &\quad + \|H_{22}^{-1} + aH_{22}^{-1}h_{21}h_{21}^\top H_{22}^{-1}\| \\ &\le |a|\|H_{22}^{-1}\|(|\bar{g}(s_0)|\|h_{21}\|^2 + 2\|h_{21}\| + \|h_{21}\|^2\|H_{22}^{-1}\|) \\ &\quad + \|H_{22}^{-1}\|, \end{aligned} \tag{A.5}$$

Using (A.2)(A.3)(A.4), we can further upper bound (A.5) as

$$\|H^{-1} - \bar{g}(s_0)e_1e_1^\top\| \le \frac{(M_1M_2 + 1)^2}{|f(s_0)|\lambda_2(L) - M_2 - M_1M_2^2}. \tag{A.6}$$

This bound holds as long as $|f(s_0)|\lambda_2(L) > M_2 + M_2^2M_1$. Combining (A.1) and (A.6) gives the desired inequality.

Appendix B. Proof of Theorems 7 and 10

When the input to the network is $U(s)$, the output response of the ith node is

$$Y_i(s) = e_i^\top T(s)U(s),$$

where e_i is the ith column of the identity matrix I_n.

Using Mellin's inverse formula (Dullerud & Paganini, 2013, Theorem 3.20), we have

$$|y_i(t) - \bar{y}(t)|$$

$$
\begin{aligned}
&= \left| \frac{1}{2\pi j} \lim_{\omega\to\infty} \int_{\sigma-j\omega}^{\sigma+j\omega} e^{st} \left(Y_i(s) - e_i^\top \bar{g}(s) \mathbb{1} \frac{\mathbb{1}^\top}{n} U(s) \right) ds \right| \\
&\le \frac{e^{\sigma t}}{2\pi} \lim_{\omega\to\infty} \int_{\sigma-j\omega}^{\sigma+j\omega} \left| e_i^\top T(s) U(s) - e_i^\top \bar{g}(s) \mathbb{1} \frac{\mathbb{1}^\top}{n} U(s) \right| ds \\
&\le \frac{e^{\sigma t}}{2\pi} \lim_{\omega\to\infty} \int_{\sigma-j\omega}^{\sigma+j\omega} \| T(s) - \frac{1}{n} \bar{g}(s) \mathbb{1}\mathbb{1}^\top \| \| U(s) \| ds \\
&= \frac{e^{\sigma t}}{2\pi} \left((A) + (B) + (C) \right),
\end{aligned}
$$

where

$$
(A) = \int_{\sigma-j\omega_0}^{\sigma+j\omega_0} \left\| T(s) - \frac{1}{n} \bar{g}(s) \mathbb{1}\mathbb{1}^\top \right\| \| U(s) \| ds,
$$

$$
(B) = \lim_{\omega\to\infty} \int_{\sigma+j\omega_0}^{\sigma+j\omega} \left\| T(s) - \frac{1}{n} \bar{g}(s) \mathbb{1}\mathbb{1}^\top \right\| \| U(s) \| ds,
$$

$$
(C) = \lim_{\omega\to\infty} \int_{\sigma-j\omega}^{\sigma-j\omega_0} \left\| T(s) - \frac{1}{n} \bar{g}(s) \mathbb{1}\mathbb{1}^\top \right\| \| U(s) \| ds.
$$

Both proofs use such a decomposition. By our assumption,

$$
\begin{aligned}
(B) &= \lim_{\omega\to\infty} \int_{\sigma+j\omega_0}^{\sigma+j\omega} \| T(s) - \frac{1}{n} \bar{g}(s) \mathbb{1}\mathbb{1}^\top \| \| U(s) \| ds \\
&\le \lim_{\omega\to\infty} \int_{\sigma+j\omega_0}^{\sigma+j\omega} \left(\| T(s) \| + \| \bar{g}(s) \| \right) \| U(s) \| ds \\
&\le 2\gamma \lim_{\omega\to\infty} \int_{\sigma+j\omega_0}^{\sigma+j\omega} \| U(s) \| ds,
\end{aligned}
$$

where the last inequality uses the fact that $\bar{g}(s)$ and $T(s)$ are stable: $\|\bar{g}(s)\|_{\mathcal{H}_\infty}, \|T(s)\|_{\mathcal{H}_\infty} \le \gamma$. Because for the real input signals, we have $U(s^*) = U^*(s)$, hence $\int_{\sigma-j\omega}^{\sigma-j\omega_0} \|U(s)\| ds = \int_{\sigma+j\omega_0}^{\sigma+j\omega} \|U(s)\| ds$, which leads to

$$
(C) \le 2\gamma \lim_{\omega\to\infty} \int_{\sigma+j\omega_0}^{\sigma+j\omega} \| U(s) \| ds.
$$

Now we are ready to prove Theorems 7 and 10.

Proof (*Proof of Theorem 7*)**.** First of all, Mellin's inverse formula requires that the vertical line $Re(s) = \sigma$ is on the right of all poles of the signal. This is the case from our assumption that $\sup_{Re(s)>\sigma} \|U(s)\| < +\infty$ and that $T(s), \bar{g}(s)$ being stable.

Given any $t \ge 0$, since $\lim_{\omega\to\infty} \int_{\sigma+j0}^{\sigma+j\omega} \|U(s)\| ds$ is finite, one can pick an $\omega_0 > 0$, such that

$$
\lim_{\omega\to\infty} \int_{\sigma+j\omega_0}^{\sigma+j\omega} \| U(s) \| ds \le \frac{2\pi\epsilon}{6e^{\sigma t}\gamma},
$$

which leads to

$$
(B) \le 2\gamma \lim_{\omega\to\infty} \int_{\sigma+j\omega_0}^{\sigma+j\omega} \| U(s) \| ds \le \frac{2\pi\epsilon}{3e^{\sigma t}}.
$$

Similarly, we have $(C) \le \frac{2\pi\epsilon}{3e^{\sigma t}}$. Notably, the choice of ω_0 depends on σt. For the remaining term, we have

$$
\begin{aligned}
(A) &= \int_{\sigma-j\omega_0}^{\sigma+j\omega_0} \| T(s) - \frac{1}{n} \bar{g}(s) \mathbb{1}\mathbb{1}^\top \| \| U(s) \| ds \\
&\le \sup_{w\in[-w_0,w_0]} \| T(\sigma+jw) - \frac{1}{n} \bar{g}(\sigma+jw) \mathbb{1}\mathbb{1}^\top \| \\
&\quad \times \int_{\sigma-j\omega_0}^{\sigma+j\omega_0} \| U(s) \| ds
\end{aligned}
$$

Since $[\sigma - j\omega_0, \sigma + j\omega_0]$ is a compact set that satisfies the assumption in Theorem 3, we have

$$
\lim_{\lambda_2(L)\to\infty} \sup_{w\in[-w_0,w_0]} \left\| T(\sigma+jw) - \frac{1}{n} \bar{g}(\sigma+jw) \mathbb{1}\mathbb{1}^\top \right\| = 0.
$$

Therefore, for a sufficiently large $\lambda_2(L)$, we have $(A) \le \frac{2\pi\epsilon}{3e^{\sigma t}}$. Combining the upperbounds for $(A), (B), (C)$, we have

$$
|y_i(t) - \bar{y}(t)| \le \epsilon.
$$

When $\sigma = 0$, notice that the choice of w_0 now does not depend on time t, thus neither does the lower bound on $\lambda_2(L)$, hence this inequality holds uniformly for all $t > 0$ with a sufficiently large $\lambda_2(L)$.

When $\sigma > 0$, the time domain bound can no longer be extended to $\{t : t > 0\}$. Nonetheless, given a $T > 0$, we have a sufficiently large $\lambda_2(L)$ such that $(A) + (B) + (C) \le \frac{2\pi\epsilon}{e^{\sigma T}}$, and this suffices to show that $\forall t \le T$,

$$
|y_i(t) - \bar{y}(t)| \le \frac{e^{\sigma t}}{2\pi} \left((A) + (B) + (C) \right) \le \frac{e^{\sigma t}}{e^{\sigma T}} \epsilon \le \epsilon.
$$

Proof (*Proof of Theorem 10*)**.** For the first scenario, the input is a sinusoidal signal $U(s) = \frac{\alpha}{s^2+\alpha^2} u_0, u_0 \in \mathbb{S}^{n-1}$ (We discuss the second scenario at the end of the proof). Mellin's inverse formula requires that the vertical line $Re(s) = \sigma$ is on the right of all poles of the signal, which is satisfied under any choice $\sigma > 0$. For our purpose, we pick

$$
\sigma = \alpha, \omega_0 = K\alpha,
$$

for some $K > 0$ (to be determined later). By our assumption,

$$
\begin{aligned}
(B) &\le 2\gamma \lim_{\omega\to\infty} \int_{\sigma+j\omega_0}^{\sigma+j\omega} \left| \frac{\alpha}{s^2+\alpha^2} \right| \| u_0 \| ds \\
&= 2\gamma \int_{\omega_0}^{+\infty} \frac{\alpha}{|(\sigma+j\omega)^2 + \alpha^2|} d\omega \\
&= 2\gamma \int_{K\alpha}^{+\infty} \frac{\alpha}{|(\alpha+j\omega)^2 + \alpha^2|} d\omega \\
&= 2\gamma \int_{K\alpha}^{+\infty} \frac{\alpha}{\sqrt{4\alpha^4 + \omega^4}} d\omega \\
&\le 2\sqrt{2}\gamma \int_{K\alpha}^{+\infty} \frac{\alpha}{2\alpha^2 + \omega^2} d\omega \\
&= \gamma \left(\pi - 2\arctan\left(\frac{K}{\sqrt{2}} \right) \right),
\end{aligned} \tag{B.1}
$$

where the last inequality uses the fact that for $a, b > 0$, we have $\sqrt{a^2+b^2} \ge (a+b)/\sqrt{2}$.

Similarly, we have

$$
(C) \le \gamma \left(\pi - 2\arctan\left(\frac{K}{\sqrt{2}} \right) \right). \tag{B.2}
$$

For the remaining term, we use the result in the proof of Theorem 4: $\exists \delta > 0$, such that $\forall s \in \mathcal{B}(0, \delta)$ such that

$$
\left\| T(s) - \frac{1}{n} \bar{g}(s) \mathbb{1}\mathbb{1}^\top \right\| \le \frac{2 (M_1 M_2 + 1)^2}{|f(s)| \lambda_2(L)},
$$

for some $M_1, M_2 > 0$. Then as long as we pick α, K appropriately such that $|\sigma + j\omega_0| \le \delta$, i.e., $\sqrt{1+K^2}\alpha \le \delta$, we have

$$
\begin{aligned}
(A) &= \int_{\sigma-j\omega_0}^{\sigma+j\omega_0} \| T(s) - \frac{1}{n} \bar{g}(s) \mathbb{1}\mathbb{1}^\top \| \left| \frac{\alpha}{s^2+\alpha^2} \right| ds \\
&\le \int_{\sigma-j\omega_0}^{\sigma+j\omega_0} \frac{2 (M_1 M_2 + 1)^2}{|f(s)| \lambda_2(L)} \left| \frac{\alpha}{s^2+\alpha^2} \right| ds
\end{aligned}
$$

$$
\begin{aligned}
&= \int_{\sigma-j\omega_0}^{\sigma+j\omega_0} \frac{2\,(M_1M_2+1)^2}{\lambda_2(L)/|s|}\frac{\alpha}{|s^2+\alpha^2|}ds \\
&= \frac{2\,(M_1M_2+1)^2}{\lambda_2(L)} \int_{\sigma-j\omega_0}^{\sigma+j\omega_0} \frac{|s|\alpha}{|s^2+\alpha^2|}ds \\
&= \frac{4\,(M_1M_2+1)^2}{\lambda_2(L)} \int_0^{K\alpha} \frac{|\alpha+j\omega|\alpha}{|(\alpha+j\omega)^2+\alpha^2|}d\omega \\
&= \frac{4\,(M_1M_2+1)^2}{\lambda_2(L)} \int_0^{K\alpha} \frac{\sqrt{\alpha^2+\omega^2}\alpha}{\sqrt{4\alpha^4+\omega^4}}d\omega \\
&\le \frac{2\sqrt{2}\,(M_1M_2+1)^2}{\lambda_2(L)} \int_0^{K\alpha} \frac{2(\alpha+\omega)\alpha}{2\alpha^2+\omega^2}d\omega,
\end{aligned}
$$

where the last equality used the fact that for $a, b > 0$, we have

$$a+b \ge \sqrt{a^2+b^2} \ge (a+b)/\sqrt{2},$$

to upper and lower bound the numerator and denominator respectively. Notice that

$$
\begin{aligned}
&\int_0^{K\alpha} \frac{2(\alpha+\omega)\alpha}{2\alpha^2+\omega^2}d\omega \\
&= \alpha\left(\sqrt{2}\arctan\left(\frac{K}{\sqrt{2}}\right) + \log\left(1+\frac{K^2}{2}\right)\right) \\
&\le 2\alpha\log\left(\frac{K^2}{2}\right), \qquad \text{(B.3)}
\end{aligned}
$$

for sufficiently large K. We have

$$(A) \le \frac{4\sqrt{2}\,(M_1M_2+1)^2}{\lambda_2(L)}\alpha\log\left(\frac{K^2}{2}\right). \qquad \text{(B.4)}$$

The last step is to find the right choice of α, K. Given $\epsilon > 0$, pick a $K > 0$, such that

$$2\gamma\left(\pi - 2\arctan\left(\frac{K}{\sqrt{2}}\right)\right) \le \frac{\epsilon\pi}{4}.$$

Generally, such a K is sufficient for (B.3) to hold. With this choice of K, let

$$\alpha_0 := \min\left\{\frac{2\log 2}{T}, \frac{\epsilon\pi\lambda_2(L)}{8\sqrt{2}(M_1M_2+1)^2\log\left(\frac{K^2}{2}\right)}, \frac{\delta}{\sqrt{1+K^2}}\right\}.$$

Then, $\forall\alpha \le \alpha_0$, combining (B.1)(B.2)(B.4), we have for any $t \le T$,

$$
\begin{aligned}
|y_i(t)-\bar{y}(t)| &\le \frac{e^{\sigma t}}{2\pi}((A)+(B)+(C)) \\
&\le \frac{e^{\alpha_0 T}}{2\pi}\left(2\gamma\left(\pi-2\arctan\left(\frac{K}{\sqrt{2}}\right)\right) + \right. \\
&\qquad \left. \frac{4\sqrt{2}\,(M_1M_2+1)^2}{\lambda_2(L)}\alpha\log\left(\frac{K^2}{2}\right)\right) \\
&\le \frac{2}{\pi}\left(\frac{\epsilon\pi}{4}+\frac{\epsilon\pi}{4}\right) = \epsilon.
\end{aligned}
$$

This finishes the proof for the first scenario. In the second scenario, the input is a convex combination of inputs that satisfies the condition in the first scenario. The results are trivial from the linearity of the system: if we denote the response of node i subjected to $\sin(\alpha_j t)\mathbf{u}_j$ as $y_i^{(j)}(t)$, then we have, for $t \le T$,

$$
\begin{aligned}
|y_i(t)-\bar{y}(t)| &= \left|\sum_j^{\infty}\beta_j y_i^{(j)}(t) - \bar{y}(t)\right| \\
&\le \sum_j^{\infty}\beta_j|y_i^{(j)}(t)-\bar{y}(t)| \le \epsilon.
\end{aligned}
$$

References

Anderson, P. M., & Mirheydar, M. (1990). A low-order system frequency response model. *IEEE Transactions on Power Systems*, *5*(3), 720–729.

Andreasson, M., Tegling, E., Sandberg, H., & Johansson, K. H. (2017). Coherence in synchronizing power networks with distributed integral control. In *IEEE 56th annu. conf. on decision and control* (pp. 6327–6333).

Bamieh, B., & Gayme, D. F. (2013). The price of synchrony: resistive losses due to phase synchronization in power networks. In *2013 American control conference* (pp. 5815–5820).

Bamieh, B., Jovanovic, M. R., Mitra, P., & Patterson, S. (2012). Coherence in large-scale networks: Dimension-dependent limitations of local feedback. *IEEE Transactions on Automatic Control*, *57*(9), 2235–2249.

Bressloff, P. C., & Coombes, S. (1999). Travelling waves in chains of pulse-coupled integrate-and-fire oscillators with distributed delays. *Physica D: Nonlinear Phenomena*, *130*(3–4), 232–254.

Chen, M. Z. Q., & Smith, M. C. (2009). A note on tests for positive-real functions. *IEEE Transactions on Automatic Control*, *54*(2), 390–393.

Chow, J. H. (1982). *Time-scale modeling of dynamic networks with applications to power systems*. Springer.

Chow, J. H. (2013). *Power system coherency and model reduction*. New York, NY, USA: Springer.

DeGroot, M. H. (1974). Reaching a consensus. *Journal of the American Statistical Association*, *69*(345), 118–121.

Dullerud, G. E., & Paganini, F. (2013). *A course in robust control theory: a convex approach*: *vol. 36*, Springer Science & Business Media.

Ekomwenrenren, E., Tang, Z., Simpson-Porco, J. W., Farantatos, E., Patel, M., & Hooshyar, H. (2021). Hierarchical coordinated fast frequency control using inverter-based resources. *IEEE Transactions on Power Systems*, *36*(6), 4992–5005.

Germond, A. J., & Podmore, R. (1978). Dynamic aggregation of generating unit models. *IEEE Transactions on Power Apparatus and Systems*, *PAS-97*(4), 1060–1069.

Ghaedsharaf, Y., Siami, M., Somarakis, C., & Motee, N. (2021). Centrality in time-delay consensus networks with structured uncertainties. *Automatica*, *125*, Article 109378.

Guggilam, S. S., Zhao, C., Dall'Anese, E., Chen, Y. C., & Dhople, S. V. (2018). Optimizing DER participation in inertial and primary-frequency response. *IEEE Transactions on Power Systems*, *33*(5), 5194–5205.

Jadbabaie, A., Lin, J., & Morse, A. (2003). Coordination of groups of mobile autonomous agents using nearest neighbor rules. *IEEE Transactions on Automatic Control*, *48*(6), 988–1001.

Jiang, Y., Bernstein, A., Vorobev, P., & Mallada, E. (2021). Grid-forming frequency shaping control in low inertia power systems. *IEEE Control Systems Letters (L-CSS)*, *5*(6), 1988–1993, also in ACC 2021.

Jiang, Y., Pates, R., & Mallada, E. (2017). Performance tradeoffs of dynamically controlled grid-connected inverters in low inertia power systems. In *56th IEEE conf. on decision and control* (pp. 5098–5105).

Jiang, Y., Pates, R., & Mallada, E. (2021). Dynamic droop control in low inertia power systems. *IEEE Transactions on Automatic Control*, *66*(8), 3518–3533.

Jönsson, U. T., & Kao, C.-Y. (2010). A scalable robust stability criterion for systems with heterogeneous LTI components. *IEEE Transactions on Automatic Control*, *55*(10), 2219–2234.

Kim, H., Shim, H., & Seo, J. (2011). Output consensus of heterogeneous uncertain linear multi-agent systems. *IEEE Transactions on Automatic Control*, *56*(1), 200–206.

Kiss, I. Z., Zhai, Y., & Hudson, J. L. (2002). Emerging coherence in a population of chemical oscillators. *Science*, *296*(5573), 1676–1678.

Lestas, I., & Vinnicombe, G. (2006). Scalable decentralized robust stability certificates for networks of interconnected heterogeneous dynamical systems. *IEEE Transactions on Automatic Control*, *51*(10), 1613–1625.

Mallada, E. (2014). *Distributed synchronization in engineering networks: the internet and electric power girds* (Ph.D. thesis), Electrical and Computer Engineering, Cornell University.

Mallada, E., Meng, X., Hack, M., Zhang, L., & Tang, A. (2015). Skewless network clock synchronization without discontinuity: Convergence and performance. *IEEE/ACM Transactions on Networking*, *23*(5), 1619–1633.

Marquez, H., & Damaren, C. (1995). Comments on "strictly positive real transfer functions revisited. *IEEE Transactions on Automatic Control*, *40*(3), 478–479.

Min, H., & Mallada, E. (2019). Dynamics concentration of large-scale tightly-connected networks. In *IEEE 58th conf. on decision and control* (pp. 758–763).

Min, H., & Mallada, E. (2021). Accurate reduced-order models for heterogeneous coherent generators. *IEEE Control Systems Letters*, *5*(5), 1741–1746.

Min, H., Pates, R., & Mallada, E. (2021). Coherence and concentration in tightly-connected networks. arXiv preprint arXiv:2101.00981.

Mirollo, R. E., & Strogatz, S. H. (1990). Synchronization of pulse-coupled biological oscillators. *SIAM Journal on Applied Mathematics*, *50*(6), 1645–1662.

Nair, S., & Leonard, N. (2008). Stable synchronization of mechanical system networks. *SIAM Journal on Control and Optimization*, *47*(2), 661–683.

Olfati-Saber, R., Fax, J. A., & Murray, R. M. (2007). Consensus and cooperation in networked multi-agent systems. *Proceedings of the IEEE*, *95*(1), 215–233.
Olfati-Saber, R., & Murray, R. (2004). Consensus problems in networks of agents with switching topology and time-delays. *IEEE Transactions on Automatic Control*, *49*(9), 1520–1533.
Oral, H. G., Mallada, E., & Gayme, D. F. (2017). Performance of first and second order linear networked systems over digraphs. In *IEEE 56th annu. conf. on decision and control* (pp. 1688–1694).
Paganini, F., & Mallada, E. (2020). Global analysis of synchronization performance for power systems: bridging the theory-practice gap. *IEEE Transactions on Automatic Control*, *65*(7), 3007–3022.
Pates, R., & Mallada, E. (2019). Robust scale-free synthesis for frequency control in power systems. *IEEE Transactions on Control of Network Systems*, *6*(3), 1174–1184.
Pirani, M., Sandberg, H., & Johansson, K. H. (2018). A graph-theoretic approach to the $\mathcal{H}_\infty$ performance of dynamical systems on directed and undirected networks. arXiv preprint arXiv:1804.10483.
Pirani, M., Shahrivar, E. M., & Sundaram, S. (2015). Coherence and convergence rate in networked dynamical systems. In *2015 54th IEEE conference on decision and control* (pp. 968–973).
Pirani, M., Simpson-Porco, J. W., & Fidan, B. (2017). System-theoretic performance metrics for low-inertia stability of power networks. In *2017 IEEE 56th annual conference on decision and control* (pp. 5106–5111).
Ramaswamy, G. N., Rouco, L., Fillatre, O., Verghese, G. C., Panciatici, P., Lesieutre, B. C., et al. (1996). Synchronic modal equivalencing (SME) for structure-preserving dynamic equivalents. *IEEE Transactions on Power Systems*, *11*(1), 19–29.
Ramaswamy, G., Verghese, G., Rouco, L., Vialas, C., & DeMarco, C. (1995). Synchrony, aggregation, and multi-area eigenanalysis. *IEEE Transactions on Power Systems*, *10*(4), 1986–1993.
Romeres, D., Dörfler, F., & Bullo, F. (2013). Novel results on slow coherency in consensus and power networks. In *2013 European control conference* (pp. 742–747).
Rudin, W., et al. (1964). *Principles of mathematical analysis*: *vol. 3*, McGraw-hill New York.
Sastry, S., & Varaiya, P. (1981). Coherency for interconnected power systems. *IEEE Transactions on Automatic Control*, *26*(1), 218–226.
Sepulchre, R., Paley, D., & Leonard, N. (2008). Stabilization of planar collective motion with limited communication. *IEEE Transactions on Automatic Control*, *53*(3), 706–719.
Siami, M., & Motee, N. (2014). Fundamental limits and tradeoffs on disturbance propagation in linear dynamical networks. *IEEE Transactions on Automatic Control*, *61*, 4055–4062.
Tegling, E., Bamieh, B., & Gayme, D. F. (2015). The price of synchrony: Evaluating the resistive losses in synchronizing power networks. *IEEE Transactions on Control of Network Systems*, *2*(3), 254–266.
Tegling, E., Bamieh, B., & Sandberg, H. (2019). Localized high-order consensus destabilizes large-scale networks. In *2019 American control conference* (pp. 760–765).
Tyuryukanov, I., Popov, M., van der Meijden, M. A. M. M., & Terzija, V. (2021). Slow coherency identification and power system dynamic model reduction by using orthogonal structure of electromechanical eigenvectors. *IEEE Transactions on Power Systems*, *36*(2), 1482–1492.
University of Edinburgh (2003). Power systems test case archive. URL https://www.maths.ed.ac.uk/optenergy/NetworkData/icelandDyn/.
Wieland, P., Sepulchre, R., & Allgöwer, F. (2011). An internal model principle is necessary and sufficient for linear output synchronization. *Automatica*, *47*(5), 1068–1074.
Wu, F., & Narasimhamurthi, N. (1983). Coherency identification for power system dynamic equivalents. *IEEE Transactions on Circuits and Systems*, *30*(3), 140–147.

Hancheng Min received his B.S. degree in automation from Tongji University, Shanghai, China, in 2016 and his M.S. degree in systems engineering from University of Pennsylvania in 2018. He received his Ph.D. degree in electrical engineering from Johns Hopkins University in 2023. He is currently a postdoc researcher at the Center for Innovation in Data Engineering and Science (IDEAS), University of Pennsylvania. His research interests include deep learning theory, analysis and control of large-scale networks, and safe reinforcement learning.

Richard Pates received the M.Eng degree in 2009, and the Ph.D. degree in 2014, both from the University of Cambridge. He is currently a Senior Lecturer at Lund University. His research interests include modular methods for control system design, stability and control of electrical power systems, and fundamental performance limitations in large-scale systems.

Enrique Mallada has been an Associate Professor of Electrical and Computer Engineering at Johns Hopkins University since 2022. Before joining Hopkins in 2016, he was a Post-Doctoral Fellow in the Center for the Mathematics of Information at Caltech from 2014 to 2016. He received his Ingeniero en Telecomunicaciones degree from Universidad ORT, Uruguay, in 2005 and his Ph.D. in Electrical and Computer Engineering with a minor in Applied Mathematics from Cornell University in 2014. Dr. Mallada has received the Johns Hopkins Alumni Association Teaching Award in 2021, the NSF CAREER award in 2018, the Center for the Mathematics of Information (CMI) Fellowship from Caltech in 2014, and the Cornell ECE Director's Ph.D. Thesis Research Award in 2014. His research interests lie in control and dynamical systems, machine learning, and optimization, with applications to safety-critical networks and systems.